Nanofocusing, shadowing, and electron mean free path in the photoemission from aerosol droplets

Author(s):
Signorell, Ruth; Goldmann, Maximilian; Yoder, Bruce L.; Bodi, Andras; Chasovskikh, Egor; Lang, Lukas; Luckhaus, David

Publication date:
2016-08-01

Permanent link:
https://doi.org/https://doi.org/10.3929/ethz-b-000117319

Originally published in:
Chemical Physics Letters 658, https://doi.org/10.1016/j.cplett.2016.05.046

Funding acknowledgement:
- Interaction of Light with Ultrafine Aerosol Particles II ()

Supplementary Information for

Nanofocusing, shadowing, and electron mean free path in the photoemission from aerosol droplets

Ruth Signorell[1,*], Maximilian Goldmann[1], Bruce L. Yoder[1], Andras Bodi[2], Egor Chasovskikh[1], Lukas Lang[1], David Luckhaus[1]

[1] *Department of Chemistry and Applied Biosciences, Laboratory of Physical Chemistry, ETH Zürich, Vladimir-Prelog-Weg 2, CH-8093, Zürich, Switzerland*

[2] *Paul Scherrer Institute, CH-5232, Villigen, Switzerland*

* To whom correspondence should be addressed. E-mail: rsignorell@ethz.ch

A. Additional Figures and Tables

Figure S1: Sketch of the experimental setup. Aerosol particles are generated either with an atomizer or nebulizer and introduced into vacuum via an aerodynamic inlet, which also acts as a size selector. The resulting beam of aerosol particles passes from the source chamber (labelled '1') to the detection chamber (labelled '2') before being photoionized by either UV or VUV light (directed perpendicular to the plane of the page, interaction volume labelled '↔'. The resulting photoelectrons are accelerated by a three plate extractor (labelled 'VMI optics') toward a position sensitive detector in a perpendicular arrangement.

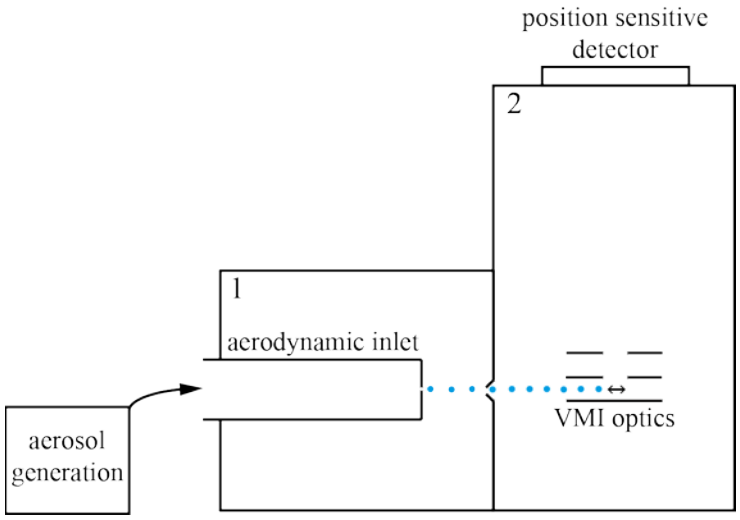

Table T1: Refractive index data of DOP. The real part *n* and imaginary part *k* of the complex index of refraction $N = n + \mathrm{i}k$ were determined from UV/VIS absorption spectra of different DOP bulk solutions using Kramers-Kronig inversion [Hawranek *et al.*, Spectrochim. Acta A, 32, 85, (1976)].

λ [nm]	*n*	*k*	λ [nm]	*n*	*k*
800	1.49	0.00	231	1.56	0.08
660	1.49	0.00	230	1.56	0.08
580	1.49	0.00	229	1.55	0.08
500	1.49	0.00	228	1.55	0.08
420	1.49	0.00	227	1.55	0.09
380	1.49	0.00	226	1.54	0.09
360	1.50	0.00	225	1.54	0.09
340	1.50	0.00	224	1.54	0.09
320	1.50	0.00	223	1.53	0.09
300	1.51	0.00	222	1.53	0.09
290	1.52	0.00	221	1.53	0.09
280	1.52	0.01	220	1.53	0.09
275	1.52	0.02	219	1.53	0.08
270	1.52	0.01	218	1.53	0.08
266	1.52	0.01	217	1.53	0.08
262	1.52	0.01	216	1.54	0.08
260	1.53	0.01	215	1.54	0.08
258	1.53	0.01	214	1.55	0.08
256	1.53	0.01	213	1.56	0.08
254	1.53	0.01	212	1.56	0.09
252	1.54	0.01	211	1.57	0.09
250	1.54	0.02	210	1.58	0.10
248	1.54	0.02	209	1.59	0.11
246	1.55	0.02	208	1.59	0.12
244	1.55	0.03	207	1.60	0.14
242	1.56	0.03	206	1.60	0.16
240	1.56	0.04	205	1.60	0.18
238	1.56	0.05	204	1.60	0.21
236	1.56	0.06	203	1.59	0.24
234	1.56	0.06	202	1.57	0.26
233	1.56	0.07	201	1.55	0.28
232	1.56	0.07	200	1.52	0.30

Figure S2: Colour map of the average of the square of the light intensity inside a 250 nm DOP droplet as a function of *n* and *k*. The local light intensities at every point inside the droplet are squared (two-photon process) and then averaged throughout the whole droplet (average of the square of the internal light intensity). The (squared) intensity of the incident light is 1. Values above 1 mean that the average internal light intensity is enhanced and values below 1 mean that the average internal light intensity is attenuated compared with the intensity of the incident light. Enhancement can only occur for very pronounced nanofocusing (here 266 nm). Shadowing always leads to light attenuation. The calculations are for a wavelength of 207 nm, but they are very similar for other wavelengths in the region between 203 and 266 nm. The black crosses qualitatively indicate the situation for the measurements shown in the left column of Figure 4 and Figure 1c and d. Note the log-scale of the colour map. The calculations were performed with the ADDA package [Yurkin *et al.*, J. Quant. Spectrosc. Radiat. Transfer, **106**, 546, (2007)].

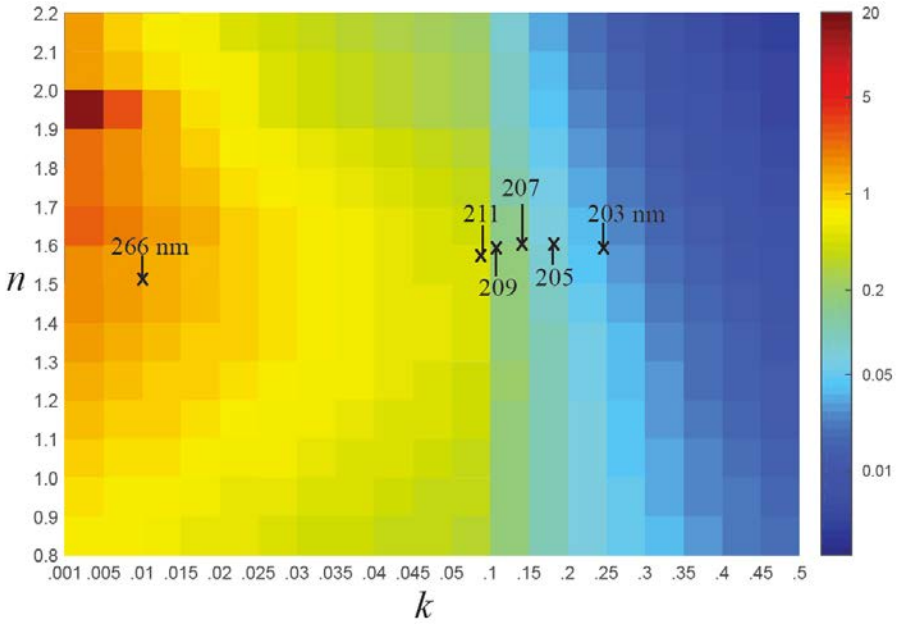

Figure S3: Histograms of the 2D velocity distribution of the photoemission from 100 nm H_2O droplets after ionization with VUV radiation of 103.3 nm. The velocity is given in mass scaled units, i. e. $\sqrt{E_{\mathrm{kin}}} = v_{\mathrm{xy}}\sqrt{m_{\mathrm{e}}/2}$ where E_{kin} is the 2D kinetic energy as indicated in the photoelectron image (Figure 5a), m_{e} is the mass of the electron and $v_{\mathrm{xy}} = \sqrt{v_x^2 + v_y^2}$ is the projection of the electron velocity onto the detector plane. (a) For the experimental photoelectron image in Figure 5a. (b) For the calculated photoelectron image in Figure 5b.

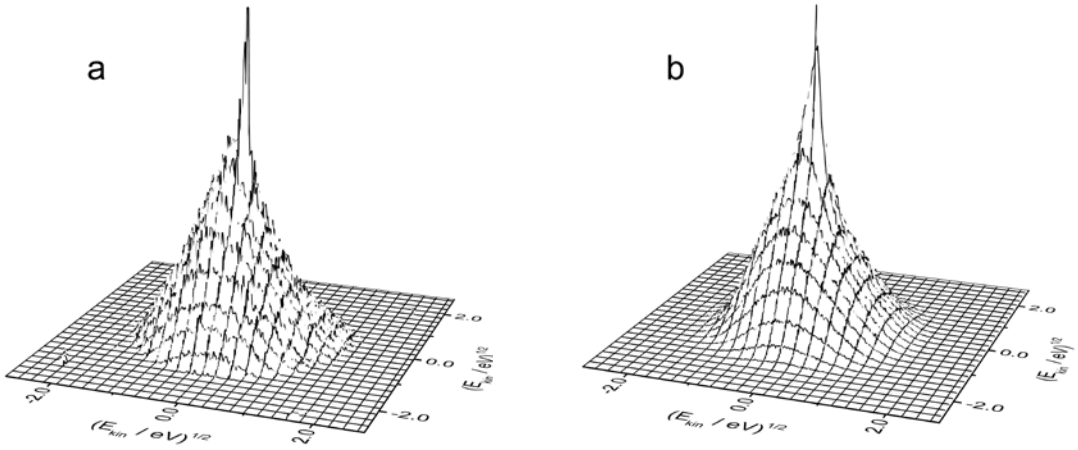

B. Description of electron transport model

The calculation of the 2D velocity distribution used an extension of the procedure outlined in ref. [Goldmann *et al.*, J. Chem. Phys., **142**, 224304, (2015)] to account for multiple scattering processes with different cross sections, energy loss functions and anisotropies. As a starting point for the refinement we employed the model proposed by Michaud, Wen and Sanche for amorphous ice [Michaud *et al.*, Radiat. Res., **159**, 3, (2003)], which we extended to lower electron kinetic energies. The nascent kinetic energy distribution of the photoelectrons was constructed so that the photoelectron spectrum at 60 eV calculated for large droplets matches the experimental data for liquid water of ref. [Winter *et al.*, J. Phys. Chem. A, **108**, 2625, (2004)] using an escape barrier of 1eV as suggested in ref. [Michaud *et al.*, Radiat. Res., **159**, 3, (2003)]. The intensity distribution we observe experimentally in the vicinity of $v_{xy} = 0$ (Figures 5 and S3) indicates a preference for inelastic forward scattering by the escape barrier for electrons that do not match the classical escape condition for a sudden barrier (instead of elastic back scattering by specular reflection as in [Goldmann *et al.*, J. Chem. Phys., **142**, 224304, (2015)]). For the current simulation we only considered the *isotropic* component of the elastic scattering cross section. The anisotropic component is dominated by forward scattering, which does not affect the distribution of photoelectrons [Michaud *et al.*, Radiat. Res., **159**, 3, (2003)]. By fitting the experimental VMI results we refined the lowest ionization energy (IE_0) with its corresponding band width (half width at half maximum, $HWHM_0$), the isotropic elastic (σ_e), and the total inelastic scattering cross section (σ_i). The energy dependence of the cross sections is described by double logarithmic interpolation of the tabulated energies quoted by Michaud, Wen and Sanche [Michaud *et al.*, Radiat. Res., **159**, 3, (2003)] with a single point added at 1.0 eV and retaining the relative contributions of the different inelastic scattering processes. We followed a two-step fitting

procedure: In a first step the overall 2D kinetic energy distribution, i.e. the VMI data integrated over the angular coordinate, was fitted, which allowed us to determine IE_0 and $HWHM_0$ while narrowing down the range of possible values for the cross sections. The latter were then refined in the second step to fit the full 2D VMI. As argued by Michaud, Wen and Sanche electron transport in liquid water is expected to be similar to that in amorphous ice, with the possible exception of the scattering off translational and librational phonons. As varying the corresponding cross sections above 1.7 eV did not significantly improve the results of the fit they were kept fixed. The final results are shown Figure S3b and Figure 5b for IE_0=10.0eV, $HWHM_0$=1.2eV, σ_e=0.6Å^2, σ_i=1.1Å^2. Including the shift by the escape barrier [Elles *et al.*, J. Chem. Phys, **125**, 044515, (2006)], IE_0 agrees well with the lowest vertical ionization energy of liquid water. The band width we obtain (with negligible contributions from the apparatus function) is consistent with the broad band observed in the liquid microjet photoelectron spectrum of water at low excitation energies [Yamamoto *et al*., J. Phys. Chem. A, **120**, 1153, (2016)]. Using these parameters we obtained the MFPs and electron attenuation lengths (EALs) given in Table 1. Note that EALs depend on the energy resolution ΔE. We define it as "the distance at which the flux of electrons maintaining the initial kinetic energy **within ΔE** diminishes by a factor of 1/e" with ΔE = 0.1eV.